Four-terminal graphene-superconductor thermal switch controlled by the superconducting phase difference

Peng-Yi Liu [1,2] Yue Mao [2] and Qing-Feng Sun [2,3,4,*]

[1] *Department of Physics, Beijing Normal University, 100875 Beijing, China*
[2] *International Center for Quantum Materials, School of Physics, Peking University, 100871 Beijing, China*
[3] *Hefei National Laboratory, Hefei, 230088 Anhui, China*
[4] *CAS Center for Excellence in Topological Quantum Computation, University of Chinese Academy of Sciences, 100190 Beijing, China*

(Received 5 July 2023; revised 23 October 2023; accepted 18 January 2024; published 1 February 2024)

We propose a superconducting phase-controlled thermal switch based on a four-terminal graphene-superconductor system. By the coupling of two superconducting leads on a zigzag graphene nanoribbon, both the normal-transmission coefficient and the crossed-Andreev-reflection coefficient, which dominate the thermal conductivity of electrons in the graphene nanoribbon, can be well controlled simultaneously by the phase difference of the superconducting leads. As a result, the thermal conductivity of electrons in the graphene nanoribbon can be tuned and a thermal switching effect appears. Using the nonequilibrium Green's function method, we verify this thermal switching effect numerically. At ambient temperatures less than about one tenth of the superconducting transition temperature, the thermal switching ratio can exceed 2000. The performance of the thermal switch can be regulated by the ambient temperature, and doping or gating can slightly increase the thermal switching ratio. The use of narrower graphene nanoribbons and wider superconducting leads facilitates the obtaining of larger thermal switching ratios. This switching effect of electronic thermal conductance in graphene is expected to be experimentally realized and applied.

DOI: 10.1103/PhysRevApplied.21.024001

I. INTRODUCTION

A heat current can carry information and energy like an electric current. Thermotronics [1], the thermal analogue of electronics, is also expected to realize effects such as thermal diodes [2–4], negative differential thermal resistance [5,6], thermal transistors [7], thermal logic gates [8,9], and thermal memory [10,11] based on heat currents. However, compared with the control of electric currents, the ability to control heat currents is much weaker. Electronics is well developed, while thermotronics started only in the last two decades [12]. In contrast to electronics, in thermal devices one does not have to worry about the serious problem of heat dissipation. In the design process for most thermal devices, it is crucial to control whether the heat current is ON or OFF, i.e., to make a thermal switch or thermal valve [13].

A thermal switch can be defined as a device that connects a high-temperature terminal (heat source) and a low-temperature terminal (heat drain). By controlling some variables of the device, one can achieve significant control over the thermal conductivity of the device [14]. Many efforts have been made in the design of thermal switches, which can control thermal conductivity through many different variables, such as temperature itself [15] and many kinds of phase transition (solid-liquid, ferromagnetic-paramagnetic, semiconductor-metal, etc.) brought about by the temperature [16–22], external electric or magnetic fields [23–28], the strain, pressure, or twist of the materials [29–32], etc. The main carriers of heat current are also different, including phonons [33], electrons [12], photons [12,34], and even magnons [35], which makes the operating temperature of thermal devices cover an enormous range from millikelvins to thousands of kelvins, which is suitable for different situations.

Superconductors are good thermal insulators at low temperatures [36], which naturally allows their application in the design of thermal devices. The study of superconducting phase-controlled thermal transport, especially for electronic thermal transport, is known as phase-coherent caloritronics [4,7,9,37–40]. Very recently, by coupling a normal lead to a notch of a superconducting ring, Ligato *et al.* [40] experimentally demonstrated that the thermal conductivity of electrons in the normal lead can be significantly controlled by the magnetic flux of the superconducting ring. Compared with other methods for thermal-switch

*sunqf@pku.edu.cn

design, since the electronic temperature evolves much faster than the phononic temperature in superconducting systems [36,38], phase-coherent caloritronics is expected to develop thermal switches that are more suitable for advanced applications, such as computing.

Graphene has attracted much attention in the last two decades due to its unique band structure [41]. Although thermal transport in graphene is phonon-dominated over a large temperature range, with decrease of the temperature and the device size, electronic thermal conductivity plays an increasingly important role [42]. Because of the weak electron-phonon coupling, at low temperature, the heat in electrons is well isolated from phonons [43–45]. So the temperature and thermal conductance of electrons in graphene can be measured and used almost unaffected by phonons. At the same time, graphene can be grown on an insulating substrate, ensuring that it is difficult for the heat of electrons to leak into the substrate. Therefore, it is possible to achieve excellent superconducting phase-controlled electronic thermal transport in a graphene-superconductor system.

In this work, using a combination of graphene and superconductors, we propose a thermal switch based on the idea of phase-coherent caloritronics. The electric transport properties of the graphene-superconductor hybrid system have been studied by many researchers, and many interesting phenomena have been exhibited, such as specular Andreev reflection (SAR) [46–49] and crossed Andreev reflection [50]. Here we study the thermal transport properties of electrons in a four-terminal graphene-superconductor system and propose a thermal-switch device. The thermal-transport properties and influencing factors of the system controlled by superconducting phase difference are analyzed theoretically and calculated numerically. By means of the nonequilibrium Green's function method, it is proved that the superconducting phase difference can remarkably control the thermal conductance of electrons in a graphene nanoribbon, and the suitable working environments are explored. From our calculations, this four-terminal structure can achieve a thermal switching ratio of more than 2000 at a low temperature with different on-site energy. In addition, the production of graphene nanoribbons with widths less than 10 nm [51,52], the high-quality contact between graphene nanoribbons and superconductors [53,54], the control of the phase difference [40,55], and the measurement of electronic temperature [34,36,40,44] are all experimentally feasible, and thus our model is realizable. The theoretical studies and numerical calculations we have performed will advance the understanding of graphene-superconductor systems and the utilization of thermotronics.

This paper is organized as follows. In Sec. II, we present the model and theory used in this paper, define the structure of the model and the Hamiltonian, and derive the specific formulas for the thermal conductance by combining the nonequilibrium Green's function method with the Landauer-Büttiker formula. In Sec. III, the numerical results are presented. On the basis of the numerical results, the ability of the superconducting phase difference to control the thermal conductance is discussed, and the effects of ambient temperature, on-site energy, and the size of the system on the thermal switching ratio are studied. Section IV concludes this paper.

II. MODEL AND FORMULATION

The thermal switching model we propose is a four-terminal graphene-superconductor system that consists of a zigzag graphene nanoribbon symmetrically coupled to two superconducting leads, as shown in Fig. 1(a). There exists a superconducting phase difference θ between the two superconducting leads. Experimentally, the two superconducting leads can be connected to form a superconducting ring, so that the phase difference can be controlled by the magnetic flux through the ring [40,55]. The phase difference can also be tuned by a supercurrent flowing through the two superconducting leads. Figure 1(b) shows the working principle of the thermal switch. A bias temperature is set so that graphene terminal 1 has a high temperature initially. When the superconducting phase difference $\theta = 0$, the thermal switch is switched off and the heat current can hardly flow from terminal 1 to terminal 3. When $\theta = \pi$, the thermal switch is switched on and the thermal conductivity is significantly increased.

Using the nearest-neighbor tight-binding method, we can express the Hamiltonian of the system as consisting of three parts [47]: $H = H_G + \sum_{\alpha=2,4}(H_{S\alpha} + H_{T\alpha})$, where H_G, $H_{S\alpha}$, and $H_{T\alpha}$ are the Hamiltonians of the graphene nanoribbon [including the dashed red box and

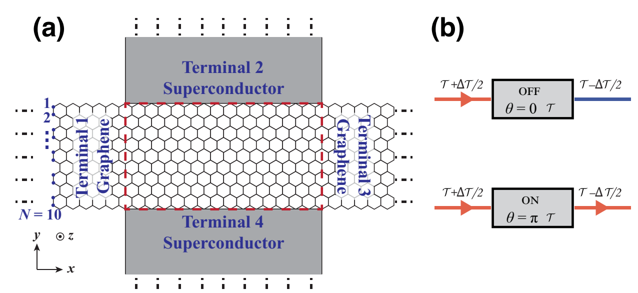

FIG. 1. (a) Graphene-superconductor four-terminal thermal switch. In this diagram, an infinite-length graphene nanoribbon is symmetrically coupled to two infinite-length superconducting leads. The width of the graphene nanoribbon $N = 10$ (N is the number of zigzag chains, which are marked on the diagram) and the width of the superconducting leads $W = 31$ (W is the number of atoms). (b) Working principle of the thermal switch. When the superconducting phase difference $\theta = 0$ ($\theta = \pi$), the heat current can hardly (easily) be transmitted from terminal 1 to terminal 3. The bias temperature between hot and cold terminals is $\Delta\mathcal{T}$, and the rest of system is at ambient temperature $\mathcal{T}$.

the graphene leads of terminals 1 and 3 in Fig. 1(a)], the superconducting leads of terminal α, and the coupling between the superconducting-lead terminal α and the graphene nanoribbon, respectively, with $\alpha = 2, 4$. They can be expressed as [47,56]

$$H_G = \sum_{i\sigma} E_0 a_{i\sigma}^\dagger a_{i\sigma} + \sum_{\langle ij\rangle\sigma} t a_{i\sigma}^\dagger a_{j\sigma}, \tag{1}$$

$$H_{S\alpha} = \sum_{\mathbf{k}\sigma} \epsilon_{\mathbf{k}} b_{\mathbf{k}\sigma,\alpha}^\dagger b_{\mathbf{k}\sigma,\alpha} + \sum_{\mathbf{k}} \left(\Delta_\alpha^* b_{\mathbf{k}\uparrow,\alpha}^\dagger b_{-\mathbf{k}\downarrow,\alpha}^\dagger + \Delta_\alpha b_{-\mathbf{k}\downarrow,\alpha} b_{\mathbf{k}\uparrow,\alpha} \right), \tag{2}$$

$$H_{T\alpha} = \sum_{i\sigma} t a_{i\sigma}^\dagger b_{i\sigma,\alpha} + \text{H.c.}, \tag{3}$$

where E_0 and t are the on-site energy and the hopping energy in the graphene region, and $a_{i\sigma}^\dagger$ ($a_{i\sigma}$) and $b_{i\sigma,\alpha}^\dagger$ ($b_{i\sigma,\alpha}$) are the creation (annihilation) operators in the graphene and the superconductor with spin $\sigma = \uparrow, \downarrow$ and site index i. The operators of the superconducting leads can be transformed between momentum space and real space, $b_{i\sigma,\alpha} = \sum_{\mathbf{k}} b_{\mathbf{k}\sigma,\alpha} e^{i\mathbf{k}\cdot\mathbf{x}_i}$, where $\mathbf{x}_i$ is the coordinate at site i. We use s-wave superconductors for the superconducting leads, with the superconducting gap $\Delta_\alpha = \Delta e^{i\phi_\alpha}$, and their phase difference $\theta = \phi_2 - \phi_4$.

According to the Landauer-Büttiker formula, the electric current and the heat current through terminal 1 can be obtained as [47,56–59]

$$I_1 = \frac{2e}{\hbar} \int \frac{dE}{2\pi} [T_{12}(f_{1e} - f_2) + T_{14}(f_{1e} - f_4) + T_{13}^A (f_{1e} - f_{3h}) + T_{11}^A (f_{1e} - f_{1h}) + T_{13}(f_{1e} - f_{3e})], \tag{4}$$

$$\dot{Q}_1 = \frac{2}{\hbar} \int \frac{dE}{2\pi} (E - \mu_1)[T_{12}(f_{1e} - f_2) + T_{14}(f_{1e} - f_4) + T_{13}^A (f_{1e} - f_{3h}) + T_{11}^A (f_{1e} - f_{1h}) + T_{13}(f_{1e} - f_{3e})], \tag{5}$$

where e and h represent an electron and a hole, respectively, and μ_1 is the chemical potential of terminal 1. We consider that a small bias voltage or a small bias temperature is applied on the graphene nanoribbon between terminal 1 and terminal 3 and the two superconductors are grounded. The Fermi distributions for the superconductor terminals are given by $f_2 = 1/[\exp(E/k_B\mathcal{T}_2) + 1]$ and $f_4 = 1/[\exp(E/k_B\mathcal{T}_4) + 1]$, and the Fermi distributions for the graphene terminals are given by $f_{1e} = 1/\{\exp[(E - eV_1)/k_B\mathcal{T}_1] + 1\}$, $f_{3e} = 1/\{\exp[(E - eV_3)/k_B\mathcal{T}_3] + 1\}$, $f_{1h} = 1/\{\exp[(E + eV_1)/k_B\mathcal{T}_1] + 1\}$, and $f_{3h} = 1/\{\exp[(E + eV_3)/k_B\mathcal{T}_3] + 1\}$, with temperature $\mathcal{T}_\alpha$ and voltage V_α. When the bias voltage ΔV and the bias temperature $\Delta\mathcal{T}$ are infinitesimal, the Fermi distribution can be approximated linearly [60]. Taking the electron as an example, we have

$$f_{\alpha e}(E) = f_0(E) - eV_\alpha \frac{\partial f_0}{\partial E} + (\mathcal{T}_\alpha - \mathcal{T}) \frac{\partial f_0}{\partial \mathcal{T}}, \tag{6}$$

where $f_0 = 1/[\exp(E/k_B\mathcal{T}) + 1]$. When we consider the electric conductance, we take $V_1 = \Delta V$, $V_2 = V_3 = V_4 = 0$, and $\mathcal{T}_1 = \mathcal{T}_2 = \mathcal{T}_3 = \mathcal{T}_4 = \mathcal{T}$. When we consider the thermal conductance, we take $\mathcal{T}_1 = \mathcal{T} + \Delta\mathcal{T}/2$, $\mathcal{T}_3 = \mathcal{T} - \Delta\mathcal{T}/2$, $V_1 = V_2 = V_3 = V_4 = 0$, and $\mu_1 = 0$. We set all parts of the system except terminals 1 and 3 to maintain the ambient temperature $\mathcal{T}$. Then we can express the electric conductance and the thermal conductance as

$$G = \frac{I_1}{\Delta V} = \frac{2e^2}{\hbar} \int \frac{dE}{2\pi} \frac{1}{k_B\mathcal{T}} \frac{\exp(E/k_B\mathcal{T})}{[\exp(E/k_B\mathcal{T}) + 1]^2} \times (T_{12} + T_{14} + T_{13} + T_{13}^A + 2T_{11}^A), \tag{7}$$

$$\kappa = \frac{\dot{Q}_1}{\Delta\mathcal{T}} = \frac{2}{\hbar} \int \frac{dE}{2\pi} \frac{E^2}{k_B\mathcal{T}^2} \frac{\exp(E/k_B\mathcal{T})}{[\exp(E/k_B\mathcal{T}) + 1]^2} \times (T_{12}/2 + T_{14}/2 + T_{13} + T_{13}^A). \tag{8}$$

The different coefficients of transmission and Andreev reflection in Eqs. (4), (5), (7), and (8) correspond to different physical processes, which can be calculated by the nonequilibrium Green's function method [47,56–58]:

(a) The normal-transmission coefficient from terminal 1 to terminal 3, $T_{13} = \mathrm{Tr}\left[\boldsymbol{\Gamma}_{1ee}\mathbf{G}_{ee}^r\boldsymbol{\Gamma}_{3ee}\mathbf{G}_{ee}^a\right]$

(b) The local-Andreev-reflection coefficient for the incident electron coming from terminal 1 with the hole Andreev-reflected to terminal 1, $T_{11}^A = \mathrm{Tr}\left[\boldsymbol{\Gamma}_{1ee}\mathbf{G}_{eh}^r\boldsymbol{\Gamma}_{1hh}\mathbf{G}_{he}^a\right]$

(c) The crossed-Andreev-reflection coefficient for the incident electron coming from terminal 1 with the hole Andreev-reflected to terminal 3, $T_{13}^A = \mathrm{Tr}\left[\boldsymbol{\Gamma}_{1ee}\mathbf{G}_{eh}^r\boldsymbol{\Gamma}_{3hh}\mathbf{G}_{he}^a\right]$

(d) The normal-transmission coefficient from terminal 1 to a superconductor terminal, $T_{12} = \mathrm{Tr}\{\boldsymbol{\Gamma}_{1ee}[\mathbf{G}^r\boldsymbol{\Gamma}_2\mathbf{G}^a]_{ee}\}$ and $T_{14} = \mathrm{Tr}\{\boldsymbol{\Gamma}_{1ee}[\mathbf{G}^r\boldsymbol{\Gamma}_4\mathbf{G}^a]_{ee}\}$

Here $\boldsymbol{\Gamma}_\alpha$ is the matrix of the linewidth function of the center region [the region surrounded by the dashed red box in Fig. 1(a)] coupled to terminal α, and $\mathbf{G}^{r(a)}$ is the matrix of the retarded (advanced) Green's function of the center region. $\boldsymbol{\Gamma}_\alpha$ and $\mathbf{G}^{r(a)}$ have been expressed in the Nambu representation, and subscripts ee, eh, he, and hh, respectively, represent the four matrix elements of Nambu subspace, with e and h for the electron and hole components.

To calculate the coefficients above, we need the matrix of the surface Green's function $\mathbf{g}_\alpha$ of each terminal, which can be obtained numerically [61]. Then, by combining the surface Green's functions with the coupling Hamiltonian between the center region and terminal α, we can calculate the retarded self-energy, whose matrix elements can be expressed as $\mathbf{\Sigma}^r_{ij,\alpha} = t g^r_{ij,\alpha} t$. The linewidth function can be obtained as $\mathbf{\Gamma}_\alpha = i[\mathbf{\Sigma}^r_\alpha - (\mathbf{\Sigma}^r_\alpha)^\dagger]$. Finally, with the Dyson equation, the retarded and advanced Green's functions of the center region can be expressed as $\mathbf{G}^r(E) = [\mathbf{G}^a(E)]^\dagger = (E\mathbf{I} - \mathbf{H}_c - \sum_{\alpha=1,2,3,4} \mathbf{\Sigma}^r_\alpha)^{-1}$, where $\mathbf{H}_c$ is the Hamiltonian of the center region.

With the formulas in this section, the electric conductance and the thermal conductance can be calculated. In the numerical calculations, we fix the superconducting gap Δ to be 1 meV, corresponding to a BCS transition temperature $T_c \approx \Delta/1.76k_B \approx 6.6$ K, which is common for conventional superconducting transition temperatures, such as for lead [62]. The hopping energy of graphene t is set to 2.75 eV as a typical value [41]. The hopping energy $t_s = 2.75$ eV and lattice constants $a_s = \sqrt{3} \times 0.142$ nm of the superconductors were selected to match the values of graphene, which leads to a BCS coherence length $\xi = \hbar v_F/\pi\Delta \approx 500$ nm similar to that in previous studies [63] and much larger than the size of our system. The Dynes broadening parameter γ [64] (i.e., the imaginary part added to the energy when we calculate the Green's function) is set to $10^{-6}\Delta$, and it can be verified that the result calculated with this value is almost the same as the results calculated with the common value of $10^{-4}\Delta$ [39,40].

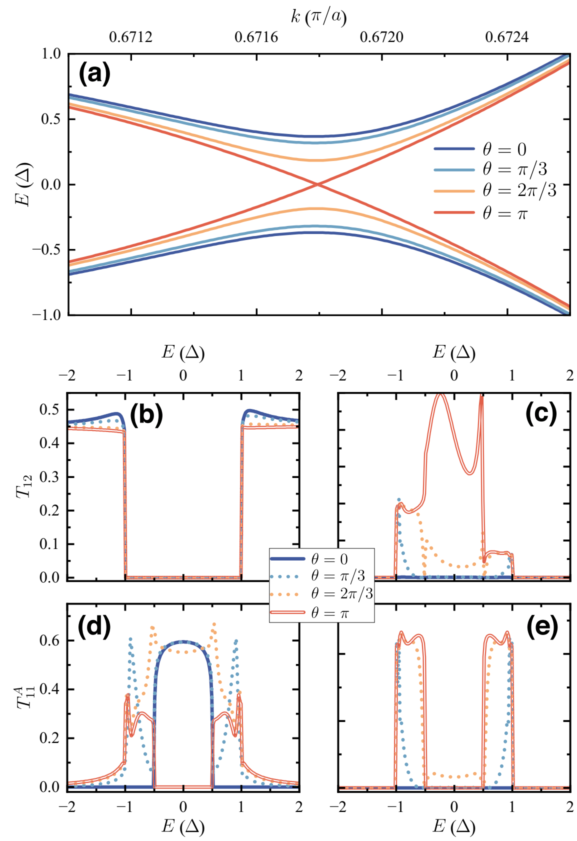

FIG. 2. Influence of superconducting phase difference θ on the energy gap and several coefficients. Here the phase difference θ is set to 0, $\pi/3$, $2\pi/3$, and π, respectively. (a) Band structure near the energy gap of the proximitized graphene. We infinitely extend the proximitized center region and the two superconductors (discrete square lattices with a width of 28 lattices) in the horizontal ($\pm\mathbf{x}$) direction to obtain the band structure. (b)–(e) Normal-transmission coefficient $T_{12}(E)$, normal-transmission coefficient $T_{13}(E)$, local-Andreev-reflection coefficient $T^A_{11}(E)$, and crossed-Andreev-reflection coefficient $T^A_{13}(E)$ versus the incident energy E, respectively. The parameters involved in the calculation are the width of the graphene nanoribbon $N = 40$, the width of the superconducting leads $W = 201$, and the on-site energy $E_0 = -0.5\Delta$.

III. RESULTS AND DISCUSSION

In this section, we report the numerical calculations for the model described in the previous section, and the control by the superconducting phase difference of the thermal conductance of the system is given. In addition, the effect of ambient temperature $\mathcal{T}$, the on-site energy E_0 (doping or gating), and the size of the center region (N, W) on the performance of the thermal switch is investigated.

In Eqs. (7) and (8), we can see that the control by the superconducting phase difference θ of the electric conductance and the thermal conductance is equivalent to the control of the transmission and Andreev-reflection coefficients. Therefore, we need to investigate the effect of the superconducting phase difference on each coefficient; the results are shown in Fig. 2. In Fig. 2(a), we present the band structure near the gap of the center graphene region [the dashed red box in Fig. 1(a)] proximitized by superconductors, which dominates the thermal switching effect. When calculating the energy band, we do not consider terminals 1 and 3, and we extend the center region and the two superconductors coupled on the upper and lower sides (a superconductor—normal-metal—superconductor junction) infinitely in the horizontal ($\pm\mathbf{x}$) direction. Here, we use the upper and lower superconductors with discrete square lattices and the 28 lattices in the y direction to provide the proximity effect. Thus, the horizontal wave vector k becomes a good quantum number to obtain the solution of the energy band. The results show that, due to the superconducting proximity effect, the band opens a gap near the Fermi surface controlled by the superconducting phase difference θ. When $\theta = 0$, the gap is the largest, while the gap is closed when $\theta = \pi$, which is consistent with the results of previous studies on superconductor—normal-metal—superconductor junctions [65]. Electrons and holes from terminal 1 need to tunnel through a barrier to move to terminal 3, when the gap is opened.

Figure 2(b) shows the normal-transmission coefficient from graphene terminal 1 to superconducting terminal 2, $T_{12}(E)$. Obviously, T_{12} appears only outside the superconducting gap Δ. The image of $T_{14}(E)$ (not given) is similar to that of $T_{12}(E)$, and because of the geometric symmetry of our system, $T_{12}(\theta) = T_{14}(-\theta)$. It can be seen that since the normal transmission into the superconductor involves only one superconducting terminal, the effect of the phase difference θ on T_{12} is not significant. The normal-transmission coefficient from graphene terminal 1 to graphene terminal 3, $T_{13}(E)$, is shown in Fig. 2(c). As the superconducting phase difference increases in $[0, \pi]$, the gap of the system gradually closes, and the height of the barrier that electrons need to tunnel through decreases [40, 65]. Therefore, T_{13} increases dramatically with increasing θ. $T_{13} \approx 0$ when $\theta = 0$, while T_{13} is close to 1 when $\theta = \pi$, which achieves a good switching effect.

Figures 2(d) and 2(e) show the coefficients of local Andreev reflection $T^A_{11}(E)$ and crossed Andreev reflection $T^A_{13}(E)$, respectively. Since our system has a joint symmetry combined by the time-reversal operator with the mirror reflection about the x-z plane or with a rotation of π about the z axis [66,67], the Andreev-reflection coefficients T^A_{11} and T^A_{13} are symmetrical about $E = 0$. With the increase of the phase difference θ in $[0, \pi]$, T^A_{11} is reduced to 0 when the incident energy $|E| \leq |E_0|$, and T^A_{13} increases from 0 for $|E_0| \leq |E| \leq \Delta$, as a result of the constructive and destructive interference of reflected holes. This is because the superconductor-graphene interface can cause both intraband ($|E| \leq |E_0|$) Andreev retroreflection (ARR) and interband ($|E_0| \leq |E| \leq \Delta$) SAR [46,68]. When $\theta = \pi$, ARR is eliminated by destructive interference and only SAR occurs. In contrast to ARR, the amplitude of SAR in a zigzag graphene nanoribbon with even chains has odd parity under mirror operation [47,69]. As a result, when $\theta = 0$, SAR is eliminated by destructive interference, and ARR reaches the maximum value. Because of the quantum diffraction effects, the reflected holes do not have definite directions, which allows holes of SAR (ARR) to also move to terminal 1 (terminal 3), leading to a nonzero value of T^A_{11} (T^A_{13}) in the region of SAR (ARR). However, considering the size of the center region, the barrier is long and multiple reflections can happen. Therefore, T^A_{13} within $|E| \leq |E_0|$ is always much smaller than 1, and increases almost monotonically with the phase difference θ in $[0, \pi]$ [see Fig. 2(e)]. In addition, T_{13} and T^A_{13} have no tail outside Δ, while T^A_{11} has a tail, which is because the first two are lost by multiple reflections during the process of reaching terminal 3.

To sum up the results in Fig. 2, the superconducting phase difference θ significantly controls T_{13}, T^A_{11}, and T^A_{13}, which mainly occur within the superconducting gap Δ. Through the control of the gap at the center region and the interference of reflected holes, T_{13} and T^A_{13} increase almost monotonically as θ increases in $[0, \pi]$. But the effect of the phase difference on T_{12} and T_{14} is weak, and occurs only outside the superconducting gap. Next, combining the coefficients with Eqs. (7) and (8), we can calculate and analyze the effect of the phase difference on the electric conductance and the thermal conductance.

In Fig. 3, we show the variation of electric conductance $G(\theta)$ and thermal conductance $\kappa(\theta)$ of electrons with the superconducting phase difference θ. It can be seen that the control by the phase difference of each coefficient does not induce a good electric switch effect. This is because the superconducting phase difference θ has opposite control effects on T^A_{11} and on T_{13} and T^A_{13}. As θ increases from 0 to π, T_{13} and T^A_{13} increase, while T^A_{11} decreases [as shown in Fig. 2(c)–2(e)]. As a result, we cannot observe the phase-controlled effect on the conductance G because G is proportional to the sum of $2T^A_{11}$, T_{13}, and T^A_{13} as shown in Eq. (7). From the physical picture, this is because Cooper pairs are able to conduct electric currents in superconductors without being restricted by the energy gap of the center region. As opposed to the conductance G, the superconducting phase difference achieves a significant on-off control of the thermal conductance at the appropriate temperature, which is similar to what was reported in recent experiments [40]. This is because as θ increases from 0 to π, both the normal-transmission coefficient T_{13} and the crossed-Andreev-reflection coefficient T^A_{13} increase: Because of the energy gap closing, T_{13} significantly increases from almost zero; because of the constructive interference of reflected holes, T^A_{13} also increases. From the physical picture, the Cooper pairs cannot conduct heat [12,36], so the thermal conductance κ is independent of the local-Andreev-reflection coefficient T^A_{11} [see Eq. (8)] and κ can be well controlled by the energy gap of the center region. In addition, it can be seen

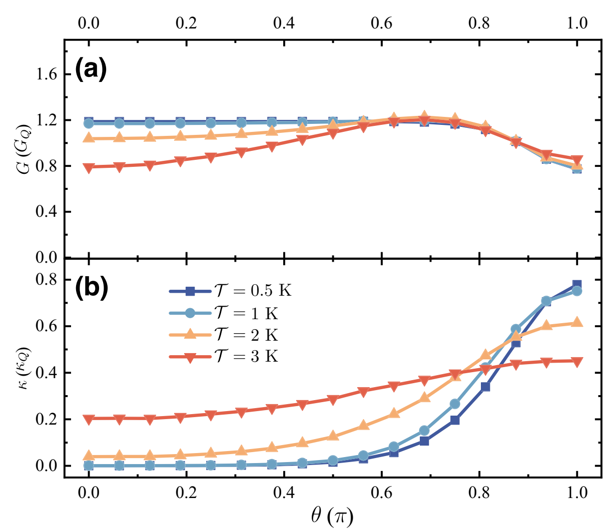

FIG. 3. (a) Electric conductance G and (b) thermal conductance κ versus superconducting phase difference θ for four different ambient temperatures: $\mathcal{T} = 0.5$, 1, 2, and 4 K. The calculated results are unitized by quantum electric conductance $G_Q = 2e^2/h$ and quantum thermal conductance $\kappa_Q = 2\pi^2 k_B^2 \mathcal{T}/3h$. The parameters involved in the calculation are the width of the graphene nanoribbon $N = 40$, the width of the superconducting leads $W = 201$, and the on-site energy $E_0 = -0.5\Delta$.

in Fig. 3(b) that ambient temperature has a great influence on the performance of the thermal switch, which can be measured by the thermal switching ratio $r = \kappa_{\max}/\kappa_{\min}$ [14]. Next, we study the influence of ambient temperature and other variables on thermal-switch performance by calculating r.

The calculated results for the thermal switching ratio varying with ambient temperature $r(\mathcal{T})$ are shown in Figs. 4(a) and 4(b). The thermal switch we devise mainly controls the heat current flowing in the graphene nanoribbon, which depends on the good thermal insulating performance of the superconductor at low temperatures [40]. As the temperature rises, the Fermi distribution widens. As a result, more electrons with energy outside Δ are involved. We already know from the above discussion that the electrons outside Δ are mainly transmitted normally into the superconductors and are hardly controlled by the phase difference, as shown in Fig. 2(b). Therefore, as shown in Figs. 4(a) and 4(b), with the increase of ambient temperature, the thermal switching ratio drops sharply for all on-site energies, which is consistent with the results of recent experiments [40]. When $\mathcal{T} \leq 1$K (about $k_B\mathcal{T} \leq \Delta/10$), the thermal switch maintains good performance. For example, the thermal switching ratio r can exceed 2000 at $\mathcal{T} = 0.5$ K, which is much larger than that given by previous thermal switches (their ratio is usually less than 100) [16,18,22,24]. Our considerations here are based on conventional superconductors ($\Delta = 1$ meV), but this device is also suitable for high-T_c superconductors. With the large energy gap of high-T_c superconductors, the sensitivity to temperature will be significantly reduced.

In contrast, the increase of $|E_0|$ not only does not harm the thermal switching effect but also slightly improves the performance of the thermal switch, and this part of the calculation results is shown in Fig. 4(c). For either normal transmission or crossed Andreev reflection, the incident electron or hole from terminal 1 needs to pass through the barrier in the center region caused by the gap in order to reach terminal 3. Since the change in the on-site energy will not have a sufficient effect on the size of the gap, our thermal switch can work over a large range of on-site energies E_0. In particular, the thermal switching ratio r can always exceed 2000 regardless of E_0 at low temperature [see the curve for $\mathcal{T} = 0.5$ K in Fig.4(c)]. Increasing $|E_0|$ can increase the density of states of graphene, which is experimentally reflected in doping or adjusting the gate voltage, to increase the carrier concentration and then to increase electronic thermal conductivity in the ON and OFF states. However, the increase of the carrier concentration also increases the superconducting proximity effect on graphene, so the control of thermal conductivity by superconductors increases as well. As shown in Fig. 4(c), with the increase of $|E_0|$, the thermal switching ratio initially (when $|E_0|$ is small) has a rapid increase and soon tends to saturation.

In addition to the case of ballistic transport, we can further consider the presence of impurities and diffusive transport caused by impurities and doping. We consider the case of Anderson disorder by adding a randomly distributed impurity potentials $w_i \in [-W_A/2, W_A/2]$ to the on-site energy in the center graphene region, i.e., $H_{\text{center}} = \sum_{i\sigma}(E_0 + w_i)a_{i\sigma}^\dagger a_{i\sigma} +$

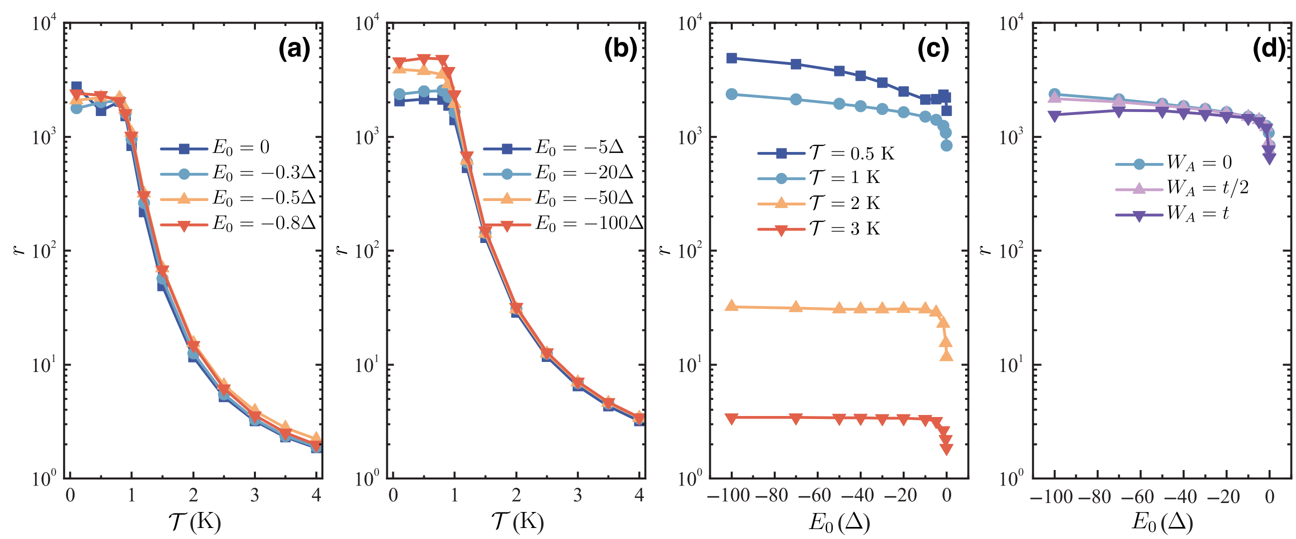

FIG. 4. (a),(b) Influence of ambient temperature $\mathcal{T}$ on the thermal switching ratio r for different on-site energies E_0. (c) Influence of on-site energy E_0 on the thermal switching ratio r at four different ambient temperatures $\mathcal{T}$. (d) Thermal switching ratio r versus on-site energy E_0 in the presence of Anderson disorder for three different disorder strengths W_A. The temperature $\mathcal{T}$ is fixed at 1 K, and each point is averaged by 200 configurations. In the calculations for (a)–(d), we used $N = 40$ for the width of the graphene nanoribbon and $W = 201$ for the width of the superconducting leads.

$\sum_{\langle ij\rangle\sigma} t a^{\dagger}_{i\sigma} a_{j\sigma}$, to simulate the effect of disorder on the system [48]. As shown in Fig. 4(d), we fix the temperature $\mathcal{T} = 1$ K, and we calculate and redraw the corresponding curve in Fig. 4(c). With the increase of the disorder strength W_A, the thermal switching ratio is slightly reduced, not surprisingly. However, the large thermal switching ratios survive even under strong disorder for $W_A = t = 2.75$ eV, which shows that the proposed thermal switch is not sensitive to disorder.

Last, we study the influence of the size of the system on the performance of the thermal switch. In the discussion of Fig. 2, we mentioned that when the phase difference $\theta = 0$, the opened energy gap becomes a barrier through which electrons and holes need to pass in the center region. The size of the system has noticeable effects on the barrier. The height of the barrier, i.e., the amplitude of the gap opening in the center region, decreases exponentially with increasing width of the graphene nanoribbon N. The barrier width is approximately equal to the width of the superconducting leads W. Therefore, decreasing N and increasing W will inhibit heat current from passing through the center region when the energy gap is open at $\theta = 0$, which will allow the thermal switch to close better. In contrast, when $\theta = \pi$, the gap closes and the barrier vanishes. In the absence of an energy gap in the center region, changing N and W will have almost no effect on the opening of the thermal switch. Therefore, the thermal switching ratio

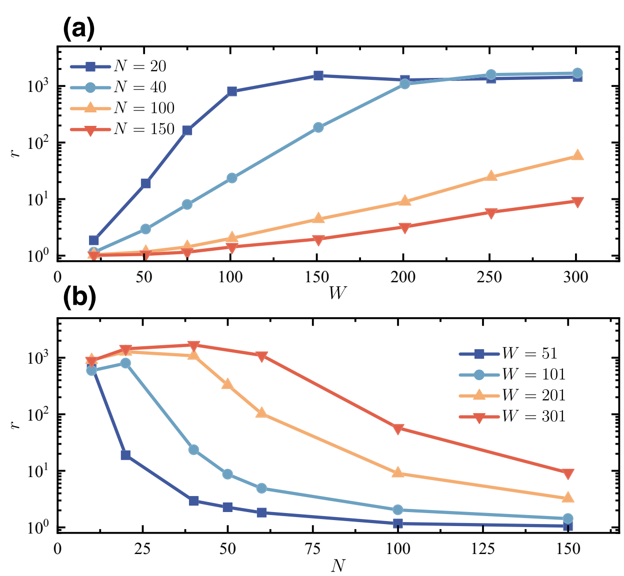

FIG. 5. Influence of the system size on the thermal switching ratio r. (a) Influence of the width W of the superconducting leads on the thermal switching ratio r for four different graphene widths N. (b) Effect of graphene width N on the thermal switching ratio r for four different widths W of the superconducting leads. The parameters involved in the calculations are the ambient temperature $\mathcal{T} = 1$ K and the on-site energy $E_0 = -0.5\Delta$.

will decrease with increasing N and increase with increasing W. Figure 5 shows the results of the calculation for variation of the system size. The variation of the thermal switching ratio is highly consistent with our analysis. In general, the choice of narrower graphene nanoribbons and wider superconducting leads allows the thermal switch to work better.

IV. CONCLUSIONS

In summary, we propose a superconducting phase-controlled thermal switch that consists of a graphene nanoribbon coupled by two superconducting leads. When the superconducting phase difference decreases from π to 0, the normal-transmission coefficient (crossed-Andreev-reflection coefficient) decreases significantly to 0 due to the opening of the energy gap (destructive interference), and then the thermal conductance of electrons in the graphene nanoribbon also decreases significantly. Using the nonequilibrium Green's function method, we verified this thermal switching effect numerically. The results show that the thermal switching ratio can exceed 2000 at ambient temperatures less than about one tenth of the superconducting transition temperature. The performance of the thermal switch can be regulated by the ambient temperature, while the increase of the carrier concentration can slightly increase the thermal switching ratio. A narrower graphene nanoribbon and wider superconducting leads are favorable for obtaining a larger thermal switching ratio. In addition, the production of graphene nanoribbons with width less than 10 nm, high-quality contact between graphene nanoribbons and superconductors, control of the superconducting phase difference, and measurement of electronic temperature are all experimentally feasible, which provides conditions for realizing our model and a high thermal switching ratio. Our work deepens the understanding of graphene-superconductor systems and provides theoretical support for research in thermotronics.

ACKNOWLEDGMENTS

This work was financially supported by the National Natural Science Foundation of China (Grants No. 12374034 and No. 11921005), the Innovation Program for Quantum Science and Technology (Grant No. 2021ZD0302403), and the Strategic Priority Research Program of the Chinese Academy of Sciences (Grant No. XDB28000000). The computational resources are supported by High-performance Computing Platform of Peking University.

[1] J. Ordonez-Miranda, Y. Ezzahri, J. A. Tiburcio-Moreno, K. Joulain, and J. Drevillon, Radiative thermal memristor, Phys. Rev. Lett. **123**, 025901 (2019).

[2] B. Li, L. Wang, and G. Casati, Thermal diode: Rectification of heat flux, Phys. Rev. Lett. **93**, 184301 (2004).
[3] C. W. Chang, D. Okawa, A. Majumdar, and A. Zettl, Solid-state thermal rectifier, Science **314**, 1121 (2006).
[4] A. Fornieri, M. J. Martínez-Pérez, and F. Giazotto, Electronic heat current rectification in hybrid superconducting devices, AIP Adv. **5**, 053301 (2015).
[5] B. Li, L. Wang, and G. Casati, Negative differential thermal resistance and thermal transistor, Appl. Phys. Lett. **88**, 143501 (2006).
[6] H.-H. Fu, D.-D. Wu, Z.-Q. Zhang, and L. Gu, Spin-dependent Seebeck effect, thermal colossal magnetoresistance and negative differential thermoelectric resistance in zigzag silicene nanoribbon heterojunciton, Sci. Rep. **5**, 10547 (2015).
[7] F. Paolucci, G. Marchegiani, E. Strambini, and F. Giazotto, Phase-tunable temperature amplifier, Europhys. Lett. **118**, 68004 (2017).
[8] L. Wang and B. Li, Thermal logic gates: Computation with phonons, Phys. Rev. Lett. **99**, 177208 (2007).
[9] F. Paolucci, G. Marchegiani, E. Strambini, and F. Giazotto, Phase-tunable thermal logic: Computation with heat, Phys. Rev. Appl. **10**, 024003 (2018).
[10] L. Wang and B. Li, Thermal memory: A storage of phononic information, Phys. Rev. Lett. **101**, 267203 (2008).
[11] V. Kubytskyi, S.-A. Biehs, and P. Ben-Abdallah, Radiative bistability and thermal memory, Phys. Rev. Lett. **113**, 074301 (2014).
[12] J. P. Pekola and B. Karimi, Colloquium: Quantum heat transport in condensed matter systems, Rev. Mod. Phys. **93**, 041001 (2021).
[13] T. Swoboda, K. Klinar, A. S. Yalamarthy, A. Kitanovski, and M. M. Rojo, Solid-state thermal control devices, Adv. Electron. Mater. **7**, 2000625 (2020).
[14] G. Wehmeyer, T. Yabuki, C. Monachon, J. Wu, and C. Dames, Thermal diodes, regulators, and switches: Physical mechanisms and potential applications, Appl. Phys. Rev. **4**, 041304 (2017).
[15] W.-R. Zhong, D.-Q. Zheng, and B. Hu, Thermal control in graphenenanoribbons: Thermal valve, thermal switch and thermal amplifier, Nanoscale **16**, 5217 (2012).
[16] R. Zheng, J. Gao, J. Wang, and G. Chen, Reversible temperature regulation of electrical and thermal conductivity using liquid–solid phase transitions, Nat. Commun. **2**, 289 (2011).
[17] B. T. Ng, Z. Y. Lim, Y. M. Hung, and M. K. Tan, Phase change modulated thermal switch and enhanced performance enabled by graphene coating, RSC Adv. **6**, 87159 (2016).
[18] K. Kim and M. Kaviany, Thermal conductivity switch: Optimal semiconductor/metal melting transition, Phys. Rev. B **94**, 155203 (2016).
[19] S. Lee, K. Hippalgaonkar, F. Yang, J. Hong, C. Ko, J. Suh, K. Liu, K. Wang, J. J. Urban, X. Zhang, C. Dames, S. A. Hartnoll, O. Delaire, and J. Wu, Anomalously low electronic thermal conductivity in metallic vanadium dioxide, Science **355**, 371 (2017).
[20] Z. Hu, M. Hiramatsu, X. He, T. Katase, T. Tadano, Keisuke Ide, H. Hiramatsu, H. Hosono, and T. Kamiya, Reversible thermal conductivity modulation of non-equilibrium $(Sn_{1-x}Pb_x)S$ by 2D–3D structural phase transition above room temperature, ACS Appl. Energy Mater. **6**, 3504 (2023).
[21] X. Zhao, J. C. Wu, Z. Y. Zhao, Z. Z. He, J. D. Song, J. Y. Zhao, X. G. Liu, X. F. Sun, and X. G. Li, Heat switch effect in an antiferromagnetic insulator $Co_3V_2O_8$, Appl. Phys. Lett. **108**, 242405 (2016).
[22] L. Castelli, Q. Zhu, T. J. Shimokusu, and G. Wehmeyer, A three-terminal magnetic thermal transistor, Nat. Commun. **14**, 393 (2023).
[23] J. F. Ihlefeld, B. M. Foley, D. A. Scrymgeour, J. R. Michael, B. Mckenzie, D. L. Medlin, M. Wallace, S. Trolier-Mckinstry, and P. E. Hopkins, Room-temperature voltage tunable phonon thermal conductivity via reconfigurable interfaces in ferroelectric thin films, Nano Lett. **15**, 1791 (2015).
[24] C. Liu, Y. Chen, and C. Dames, Electric-field-controlled thermal switch in ferroelectric materials using first-principles calculations and domain-wall engineering, Phys. Rev. Appl. **11**, 044002 (2019).
[25] B. M. Foley, M. Wallace, J. T. Gaskins, E. A. Paisley, R. L. Johnson-Wilke, J. W. Kim, P. J. Ryan, S. Trolier-Mckinstry, P. E. Hopkins, and J. F. Ihlefeld, Voltage-controlled bistable thermal conductivity in suspended ferroelectric thin-film membranes, ACS Appl. Mater. Interfaces **10**, 25493 (2018).
[26] A. N. McCaughan, V. B. Verma, S. M. Buckley, J. P. Allmaras, A. G. Kozorezov, A. N. Tait, S. W. Nam, and J. M. Shainline, A superconducting thermal switch with ultrahigh impedance for interfacing superconductors to semiconductors, Nat. Electron. **2**, 451 (2019).
[27] H. T. Huang, M. F. Lai, Y. F. Hou, and Z. H. Wei, Influence of magnetic domain walls and magnetic field on the thermal conductivity of magnetic nanowires, Nano Lett. **15**, 2773 (2015).
[28] R. Bosisio, S. Valentini, F. Mazza, G. Benenti, R. Fazio, V. Giovannetti, and F. Taddei, Magnetic thermal switch for heat management at the nanoscale, Phys. Rev. B **91**, 205420 (2015).
[29] X. Liu, G. Zhang, and Y. W. Zhang, Graphene-based thermal modulators, Nano Res. **8**, 2755 (2015).
[30] Y. Zeng, C.-L. Lo, S. Zhang, and Z. Chen, Dynamically tunable thermal transport in polycrystalline graphene by strain engineering, Carbon **158**, 63 (2020).
[31] A. Ott, Y. Hu, X.-H. Wu, and S.-A. Biehs, Radiative thermal switch exploiting hyperbolic surface phonon polaritons, Phys. Rev. Appl. **15**, 064073 (2021).
[32] Y. Du, J. Peng, Z. Shi, and J. Ren, Twist-induced near-field radiative heat switch in hyperbolic antiferromagnets, Phys. Rev. Appl. **19**, 024044 (2023).
[33] N. Li, J. Ren, L. Wang, G. Zhang, P. Hänggi, and B. Li, Colloquium: Phononics: Manipulating heat flow with electronic analogs and beyond, Rev. Mod. Phys. **84**, 1045 (2012).
[34] A. Ronzani, B. Karimi, J. Senior, Y.-C. Chang, J. T. Peltonen, C. Chen, and J. P. Pekola, Tunable photonic heat transport in a quantum heat valve, Nat. Phys. **14**, 991 (2018).
[35] R. Jin, Y. Onose, Y. Tokura, D. Mandrus, P. Dai, and B. C. Sales, In-plane thermal conductivity of Nd_2CuO_4:

Evidence for magnon heat transport, Phys. Rev. Lett. **91**, 146601 (2003).
[36] F. Giazotto, T. T. Heikkilä, A. Luukanen, A. M. Savin, and J. P. Pekola, Opportunities for mesoscopics in thermometry and refrigeration: Physics and applications, Rev. Mod. Phys. **78**, 217 (2006).
[37] A. Fornieri and F. Giazotto, Towards phase-coherent caloritronics in superconducting circuits, Nat. Nanotechnol. **12**, 944 (2017).
[38] C. Guarcello, P. Solinas, A. Braggio, M. Di Ventra, and F. Giazotto, Josephson thermal memory, Phys. Rev. Appl. **9**, 014021 (2018).
[39] E. Strambini, F. S. Bergeret, and F. Giazotto, Proximity nanovalve with large phase-tunable thermal conductance, Appl. Phys. Lett. **105**, 082601 (2014).
[40] N. Ligato, F. Paolucci, E. Strambini, and F. Giazotto, Thermal superconducting quantum interference proximity transistor, Nat. Phys. **18**, 627 (2022).
[41] A. H. Castro Neto, F. Guinea, N. M. R. Peres, K. S. Novoselov, and A. K. Geim, The electronic properties of graphene, Rev. Mod. Phys. **81**, 109 (2009).
[42] T. Y. Kim, C.-H. Park, and N. Marzari, The electronic thermal conductivity of graphene, Nano Lett. **16**, 2439 (2016).
[43] J. K. Viljas and T. T. Heikkilä, Electron-phonon heat transfer in monolayer and bilayer graphene, Phys. Rev. B **81**, 245404 (2010).
[44] K. C. Fong and K. C. Schwab, Ultrasensitive and wide-bandwidth thermal measurements of graphene at low temperatures, Phys. Rev. X **2**, 031006 (2012).
[45] S. Yiğen, V. Tayari, J. O. Island, J. M. Porter, and A. R. Champagne, Electronic thermal conductivity measurements in intrinsic graphene, Phys. Rev. B **87**, 241411(R) (2013).
[46] C. W. J. Beenakker, Specular Andreev reflection in graphene, Phys. Rev. Lett. **97**, 067007 (2006).
[47] S.-G. Cheng, Y. Xing, J. Wang, and Q.-F. Sun, Controllable Andreev retroreflection and specular Andreev reflection in a four-terminal graphene-superconductor hybrid system, Phys. Rev. Lett. **103**, 167003 (2009).
[48] S.-G. Cheng, H. Zhang, and Q.-F. Sun, Effect of electron-hole inhomogeneity on specular Andreev reflection and Andreev retroreflection in a graphene-superconductor hybrid system, Phys. Rev. B **83**, 235403 (2011).
[49] Q. Cheng and Q.-F. Sun, Specular Andreev reflection and its detection, Phys. Rev. B **103**, 144518 (2021).
[50] W.-T. Lu and Q.-F. Sun, Electrical control of crossed Andreev reflection and spin-valley switch in antiferromagnet/superconductor junctions, Phys. Rev. B **104**, 045418 (2021).
[51] X. Li, X. Wang, L. Zhang, S. Lee, and H. Dai, Chemically derived, ultrasmooth graphene nanoribbon semiconductors, Science **319**, 1229 (2008).
[52] J. W. Bai, X. F. Duan, and Y. Huang, Rational fabrication of graphene nanoribbons using a nanowire etch mask, Nano Lett. **9**, 2083 (2009).
[53] F. Miao, S. Wijeratne, Y. Zhang, U. C. Coskun, W. Bao, and C. N. Lau, Phase-coherent transport in graphene quantum billiards, Science **317**, 1530 (2007).
[54] F. Amet, C. T. Ke, I. V. Borzenets, J. Wanf, K. Watanabe, T. Taniguchi, R. S. Deacon, M. Yamamoto, Y. Bomze, S. Tarucha, and G. Finkelstein, Supercurrent in the quantum Hall regime, Science **352**, 966 (2016).
[55] F. Giazotto, J. T. Peltonen, M. Meschke, and J. P. Pekola, Superconducting quantum interference proximity transistor, Nat. Phys. **6**, 254 (2010).
[56] Q.-F. Sun and X. C. Xie, Quantum transport through a graphene nanoribbon–superconductor junction, J. Phys.: Condens. Matter **21**, 344204 (2009).
[57] Y. Meir and N. S. Wingreen, Landauer formula for the current through an interacting electron region, Phys. Rev. Lett. **68**, 2512 (1992).
[58] A.-P. Jauho, N. S. Wingreen, and Y. Meir, Time-dependent transport in interacting and noninteracting resonant-tunneling systems, Phys. Rev. B **50**, 5528 (1994).
[59] N.-X. Yang, Q. Yan, and Q.-F. Sun, Half-integer quantized thermal conductance plateau in chiral topological superconductor systems, Phys. Rev. B **105**, 125414 (2022).
[60] M.-M. Wei, Y.-T. Zhang, A.-M. Guo, J.-J. Liu, Y. Xing, and Q.-F. Sun, Magnetothermoelectric transport properties of multiterminal graphene nanoribbons, Phys. Rev. B **93**, 245432 (2016).
[61] D. H. Lee and J. D. Joannopoulos, Simple scheme for surface-band calculations. II. The Green's function, Phys. Rev. B **23**, 4997 (1981).
[62] N. W. Ashcroft and N. D. Mermin, *Solid State Physics* (Holt, Rinehart and Winston, New York, 1976).
[63] G.-H. Lee and H.-J. Lee, Proximity coupling in superconductor-graphene heterostructures, Rep. Prog. Phys. **81**, 056502 (2018).
[64] R. C. Dynes, J. P. Garno, G. B. Hertel, and T. P. Orlando, Tunneling study of superconductivity near the metal-insulator transition, Phys. Rev. Lett. **53**, 2437 (1984).
[65] H. le Sueur, P. Joyez, H. Pothier, C. Urbina, and D. Esteve, Phase controlled superconducting proximity effect probed by tunneling spectroscopy, Phys. Rev. Lett. **100**, 197002 (2008).
[66] Q. Cheng, Q. Yan, and Q.-F. Sun, Spin-triplet superconductor–quantum anomalous Hall insulator–spin-triplet superconductor Josephson junctions: 0–π transition, ϕ_0 phase, and switching effects, Phys. Rev. B **104**, 134514 (2021).
[67] W.-T. Lu and Q.-F. Sun, Spin polarization and Fano–Rashba resonance in nonmagnetic graphene, New J. Phys. **25**, 043018 (2023).
[68] C. W. J. Beenakker, Colloquium: Andreev reflection and Klein tunneling in graphene, Rev. Mod. Phys. **80**, 1337 (2008).
[69] Y. Xing, J. Wang, and Q.-F. Sun, Parity of specular Andreev reflection under a mirror operation in a zigzag graphene ribbon, Phys. Rev. B **83**, 205418 (2011).